Kinetic Energy of a Disabled Quadcopter Upon Impact at Terminal Velocity

by
Z. A. Sechrist, PhD; J. P. Mondragon; G. T. Ewing; R. G. Snyder;
P. M. Charles, Jr..; B. K. Pate; T. D. Heston;
W. S. Thompson; M. A. Ramirez
Technical Analysis Group
Naval Air Warfare Center Weapons Division (NAWCWD)
China Lake, CA

J. W. Sumners; S. T. Selph
Quick Reaction Capabilities Office
China Lake Ranges Department
NAWCWD, China Lake, CA

J. C. Little; R. J. Tonucci, PhD; T. C. Clutz, PhD
Defense Threat Reduction Agency (DTRA)
Fort Belvoir, VA

APRIL 2021

NAVAL AIR WARFARE CENTER WEAPONS DIVISION
CHINA LAKE, CA 93555-6100

Naval Air Warfare Center Weapons Division

FOREWORD

This final report describes the test procedures, results, and analysis of a test bed designed to investigate the danger posed by disabled quadcopter unmanned aerial vehicles striking a person. The use of quadcopters in hobby, commercial, and nefarious activities has surged in recent years, and the safety risks posed by this new technology exist. This effort informs guidance for organizations responsible to responding to quadcopter unmanned aerial vehicles as a threat, as well as delivers a scientific evaluation of the risks generated if counter-unmanned aerial vehicle weapons must be used.

This work was executed by the Naval Air Warfare Center Weapons Division (NAWCWD) China Lake's cross-competency Technical Analysis Group from October 2018 to December 2018 under the sponsorship of the Joint Improvised-Threat Defeat Organization (JIDO), now known as part of the Defense Threat Reduction Agency (DTRA).

This report was reviewed for technical accuracy by Mark A. Ramirez.

Approved by
D. W. HORNING, *Director for Weapons*
Weapons and Energetics Department
8 April 2021

Under authority of
W. S. DILLON
RDML, U.S. Navy
Commander

Released for publication by
D. A. CARREÑO
Director for Research and Engineering

NAWCWD Technical Publication 8855

Published by ..... Technical Communications and Graphics Branch
Collation ..... Cover, 11 leaves
First printing ..... 1 paper, 4 electronic media

REPORT DOCUMENTATION PAGE

Form Approved
OMB No. 0704-0188

1. REPORT DATE *(DD-MM-YYYY)*	2. REPORT TYPE	3. DATES COVERED (From - To)
08-04-2021	Final	1 October – 31 December 2018

4. TITLE AND SUBTITLE
Kinetic Energy of a Disabled Quadcopter Upon Impact at Terminal Velocity (U)

5a. CONTRACT NUMBER
N/A

5b. GRANT NUMBER
N/A

5c. PROGRAM ELEMENT NUMBER
N/A

6. AUTHOR(S)
Z. A. Sechrist, PhD; J. P. Mondragon; G. T. Ewing; R. G. Snyder; P. M. Charles, Jr..; B. K. Pate; T. D. Heston; W. S. Thompson; M. A. Ramirez; J. W. Sumners; S. T. Selph (NAWCWD)

J. C. Little; R. J. Tonucci, PhD; T. C. Clutz, PhD (DTRA)

5d. PROJECT NUMBER
N/A

5e. TASK NUMBER
N/A

5f. WORK UNIT NUMBER
N/A

7. PERFORMING ORGANIZATION NAME(S) AND ADDRESS(ES)
Technical Analysis Group
Naval Air Warfare Center Weapons Division
1 Administration Circle
China Lake, California 93555-6100

8. PERFORMING ORGANIZATION REPORT NUMBER
NAWCWD TP 8855

9. SPONSORING/MONITORING AGENCY NAME(S) AND ADDRESS(ES)
Defense Threat Reduction Agency RD-ECT
(formerly the Joint Improvised-Threat Defeat Organization [JIDO])
8725 John J. Kingman Road, Mail Stop 6201
Fort Belvoir, Virginia 22060-6201

10. SPONSOR/MONITOR'S ACRONYM(S)
DTRA

11. SPONSOR/MONITOR'S REPORT NUMBER(S)
N/A

12. DISTRIBUTION/AVAILABILITY STATEMENT
DISTRIBUTION STATEMENT A. Approved for public release; distribution is unlimited.

13. SUPPLEMENTARY NOTES
None.

14. ABSTRACT

(U) The risk posed by a head strike from a disabled quadcopter was investigated in terms of kinetic energy and impact area. The experiments compared components of, and intact, DJI Phantom 4 Pro. The types of counter-unmanned aerial vehicle disabling mechanisms considered in the paper included propeller entanglement, motor shutdown, and structural breakup. The quadcopter disabled through a motor shutdown mechanism displayed windmilling as they fell. The windmilling effect decreased the velocity, and therefore kinetic energy, of the quadcopter at impact. Windmilling also oriented the quadcopter during descent such that the quadcopter fell in an upright position such that impact occurred on the deformable/frangible landing gear. The landing gear and other plastic components of the quadcopter showed multiple permanent breaks and bends that would absorb energy of an impact. Disablement via propeller entanglement led to higher impact velocity and more quadcopter rotation compared to motor shutdown. Structural breakup posed an increased risk because that type of disablement multiplies the number of dangerous objects that could cause fatal injury, where the resulting rigid/robust falling objects would efficiently transfer energy during an impact.

15. SUBJECT TERMS
Blunt Criterion, Collateral Damage, Counter-Unmanned Aerial Vehicle (CUAV), Disabled, Hazard, Quadcopter, Risk, Unmanned, Windmilling

16. SECURITY CLASSIFICATION OF:			17. LIMITATION OF ABSTRACT	18. NUMBER OF PAGES	19a. NAME OF RESPONSIBLE PERSON
a. REPORT	b. ABSTRACT	c. THIS PAGE			Zachary Sechrist
UNCLASSIFIED	UNCLASSIFIED	UNCLASSIFIED	SAR	20	19b. TELEPHONE NUMBER *(include area code)* (760) 696-2090

CONTENTS

Tables:

INTRODUCTION

The purchase and use of unmanned aerial vehicles (UAVs) has grown rapidly during recent years. The Federal Aviation Administration (FAA) reported 626,245 hobbyist UAVs were registered in 2016 (the first year for an FAA rule requiring UAV registration and predicts the UAV fleet in the US to be between 2.75 to 4.47 million hobbyist units by 2021 (Reference 1). While a majority of these units will be used legally, multiple news stories have surfaced about UAVs being used for nefarious applications, such as weaponized UAV attacks, witness intimidation, contraband delivery, airport disruption, and emergency service disruption (References 2 through 6). Due to the inevitable misuse of burgeoning UAV technology, it is valuable to consider the types of counter-UAV (CUAV) weapons available and the potential threat of collateral damage posed by a UAV disabled after a successful engagement by a CUAV weapon.

A successful CUAV weapon attack would cause the UAV to experience an uncontrolled descent. Only UAV disabling technologies were considered in this study, not corruption of the radio frequency link between the controller and UAV. It is believed that disabling CUAV weapons can be broadly grouped into three categories:

1. Propeller entanglement
2. Motor shutdown
3. Structural breakup

Propeller entanglement involves the physical binding of the UAV's propellers by a net, string, or highly viscous fluid. The entanglement mechanism may not break any parts off the UAV but does prevent the propellers from spinning. The motor shutdown category includes any attack that stops the motors from driving the propellers without binding the propellers or creating significant UAV breakup. Weapons capable of motor shutdown include high-power microwave directed energy attack or a small-caliber projectile or laser strike that disrupts the electrical system without physical separation of any major components of an airborne UAV. The UAV structural breakup is caused by a large-caliber projectile, multiple small-caliber projectiles, UAV-on-UAV collision, an onboard fire, or a pressure wave that physically breaks the UAV into its constituent pieces. This study did not investigate the possible collateral damage threat generated by the rounds fired by the CUAV weapon, only the potential threat posed by the UAV after the disabling attack had occurred.

Several research groups have previously investigated the threat posed by a collision of a person with a quadcopter UAV (References 7 through 20). This study expanded on previous work by comparing the threat of individual components in/on the UAV in addition to an intact UAV. The components, as well as the intact UAV, were tested as falling objects resulting from a CUAV attack. This study compared the kinetic energy from the following items accelerated to terminal velocity: intact quadcopter UAV, quadcopter UAV with bound propellers, quadcopter UAV with propellers removed, quadcopter UAV shell, battery only, motor only, camera only, and a quadcopter UAV with a custom payload. This

study investigated the fall time of each subject under test (SUT) covering a 96-foot test bed and then extrapolated that fall time to predict the terminal velocity that each SUT would be able to achieve. The mass and terminal velocity were used to predict the kinetic energy that each SUT would have upon impact at terminal velocity. The Blunt Criterion (BC) trauma model was used to quantify the blunt force trauma head injury threat to people from the disabled quadcopter UAV (or components of UAV). The applicability of the BC method is discussed for each SUT.

EXPERIMENT

SUTs

All tests were performed with a DJI Phantom 4 Pro quadcopter or components from a Phantom 4 Pro. This platform was chosen as the "typical" quadcopter UAV based on FAA registration data published in 2017. At that time, the FAA required non-hobbyists to register each UAV that would be flown, allowing for a brand/type analysis. A statistical analysis of published non-hobbyist FAA registrations reported that the DJI Phantom 4 Pro was the most popular UAV registered, followed by the closely related DJI Phantom 3 (Reference 21). A DJI Phantom 4 Pro quadcopter and the additional variants of that platform tested herein are shown in Figure 1.

The UAV was modified with a cable tie loop above the center of the UAV that was used to hold the UAV prior to each test drop, and a piece of reflective tape on a single arm that helped researchers track any rotation during the uncontrolled fall.

(a) Phantom 4 Pro with free-spinning propellers.

(b) Phantom 4 Pro with bound propellers.

(c) Phantom 4 Pro without propellers.

(d) Payload-burdened Phantom 4 Pro with free-spinning propellers.

(e) Payload-burdened Phantom 4 Pro with bound propellers.

(f) Payload-burdened Phantom 4 Pro without propellers.

(g) Phantom 4 Pro shell.

(h) DJI camera.

(i) DJI propeller.

(j) DJI battery.

(k) DJI motor.

FIGURE 1. SUTs.

TEST BED

An indoor test facility was chosen to eliminate wind effects and generate a controlled landing site for the falling disabled UAVs and/or components. A schematic of the test bed used for fall time analysis is shown in Figure 2.

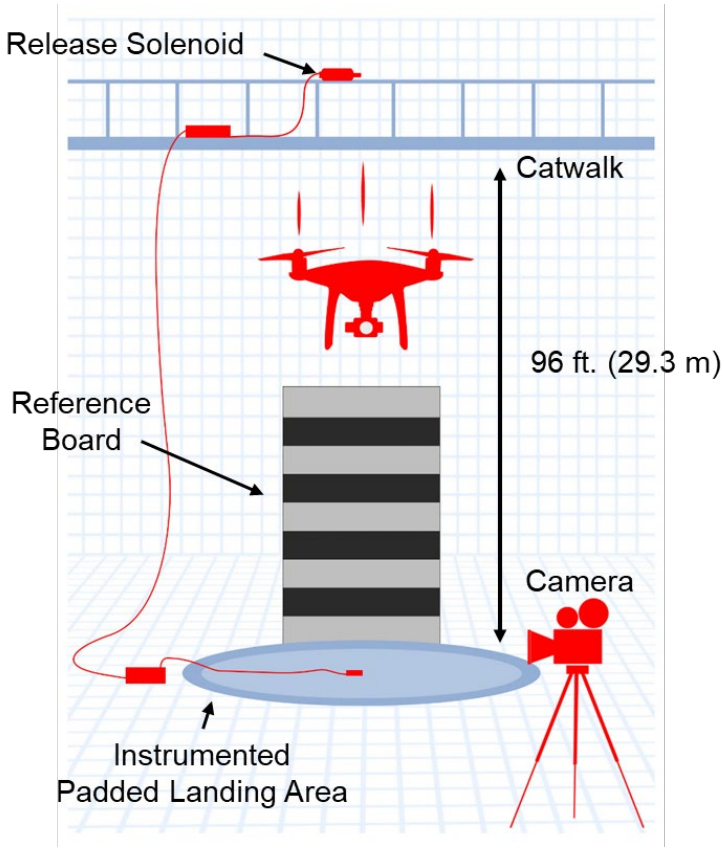

FIGURE 2. UAV Fall Time Test Bed (Not Drawn to Scale).

The falling UAVs were filmed with a Sony RX10 III camera operating at 480 frames per second. The SUT was suspended by a cable tie loop held onto a solenoid shaft. When the release switch was triggered, the solenoid shaft was retracted, and the SUT fell down to the instrumented landing pad. The SUT had no initial velocity prior to the drop. The landing pad consisted of a taut 6-ft-by-6-ft (1.8-m-by-1.8-m) tarpaulin over a bed of 10-in-by-10-in-by-10-in (25.4-cm-25.4-cm-by-25.4-cm) foam cubes contained in a 15-foot (4.5-meter) diameter netted trampoline. Impact with the tarpaulin was measured with a MPU-6050 three-axis accelerometer, a three-axis gyroscope fixed to the tarpaulin, and a trip wire that broke electrical contact when the tarp was pulled. Arduino Uno microcontrollers monitored the solenoid trigger and the landing pads sensors as a function of time. Timing collected from the two sensors were in good agreement with each other.

TERMINAL VELOCITY ESTIMATION

The 96-foot (29.3-meter) fall distance in the available test bed was not long enough to reach terminal velocity. The fall time recorded for each SUT was measurably greater than the time predicted for free fall without drag. The retarded fall time of the UAV and components was used to estimate the drag coefficient and projected area of each SUT, which was in turn used to estimate the terminal velocity of the falling SUT. It was assumed

that no additional flight termination system, such as a parachute, would be active on the SUT.

The quadratic equation of motion (Equation 1) was used to relate the measured time and fixed fall distance to an acceleration:

$$x(t) = x_0 + v_0 * t + \frac{1}{2} * a * t^2 \quad (1)$$

where $x(t)$ is position at time t, x_0 is position at time = 0, v_0 is velocity at time = 0, and a is acceleration, t is time. The initial position and initial velocity were zero. The acceleration experienced by the falling SUT was due to both gravitational and drag forces as shown in Equation 2:

$$a = g - \frac{D}{m} \quad (2)$$

where g is acceleration due to gravity, D is drag force, and m is mass of the falling object. Assuming the gravitational force was constant allowed solving for the drag force using the fall distance and time. Equation 3 was used as the governing equation for an iterative fit process in Microsoft Excel that delivered the product of drag coefficient and projected area for each SUT based on the drag force for each object:

$$D = \frac{1}{2} * C_d * A * \rho * v^2 \quad (3)$$

where v is velocity at time t, A is projected area of the falling object, ρ is density of air, and C_d is drag coefficient. Once the product of drag coefficient and projected area were known for the SUT, Equation 4 was used to solve for the terminal velocity of the SUT:

$$v_{terminal} = \left(\frac{2 * m * g}{\rho * C_d * A}\right)^{\frac{1}{2}} \quad (4)$$

The kinetic energy (KE) at terminal velocity for each SUT was then calculated by inserting the estimated terminal velocity into the familiar kinetic energy definition shown in Equation 5:

$$KE = \frac{1}{2} * m * v_{terminal}{}^2 \quad (5)$$

RESULTS AND DISCUSSION

FALL TIME

Table 1 shows the fall times and resulting kinetic energy of each SUT examined in this study. The fall times were the average of five SUT drop experiments over the 96-foot (29.3-meter) test bed. As expected, all of the objects had fall times greater than the time predicted for an object in free fall (no drag force)—2.44 seconds. The detached propeller had the longest fall time. The DJI battery had the shortest fall time. The low drag battery, motor, and quadcopters without propellers all had similar fall times.

TABLE 1. Fall Times, Volume, Mass, Estimated Terminal Velocity, Required Fall Distance to Achieve Terminal Velocity and Kinetic Energy of Falling Objects.

Falling Object	Volume, in^3 (cm^3)	Mass, lb (kg)	Fall Time, s	Terminal Velocity, ft/s (m/s)	Fall Distance for 98% Term. Velocity, ft (m)	Kinetic Energy, ft-lb (N-m)
Intact UAV – free-spinning propellers	91 (1,491.2)	3.02 (1.4)	2.71	69 (21.0)	242 (73.7)	225 (305.1)
Intact UAV – 4 bound propellers	91 (1,491.2)	3.03 (1.4)	2.64	80 (24.4)	324 (98.8)	305 (413.5)
UAV – no propellers	88 (1,442.1)	2.92 (1.3)	2.58	96 (29.3)	465 (141.7)	419 (568.1)
DJI motor	1 (16.4)	0.12 (0.05)	2.56	104 (31.7)	541 (164.9)	20 (27.1)
DJI battery	21 (344.1)	1.02 (0.5)	2.54	114 (34.7)	652 (198.7)	205 (277.9)
DJI camera	7 (114.7)	0.41 (0.2)	2.71	69 (21.0)	242 (73.7)	30 (40.7)
DJI shell	82 (1,343.7)	1.02 (0.5)	2.69	72 (21.9)	260 (79.2)	82 (111.2)
DJI propeller	1 (16.4)	0.02 (0.009)	4.08	27 (8.2)	38 (11.6)	0.3 (0.41)
UAV with payload – free-spinning propellers	109 (1,786.2)	3.68 (1.7)	2.67	75 (22.9)	284 (86.6)	322 (436.6)
UAV with payload – 4 bound propellers	109 (1,786.2)	3.68 (1.7)	2.59	93 (28.3)	434 (132.3)	493 (668.4)
UAV with payload – no propellers	106 (1,737.0)	3.58 (1.6)	2.54	114 (34.7)	652 (198.7)	720 (976.2)

MINIMUM FALL DISTANCE FOR TERMINAL VELOCITY

The velocity as a function of fall distance asymptotically approaches terminal velocity, so the distance required to reach 98% (rather than 100%) of the terminal velocity was reported in Table 1 to give the reader an approximate UAV flight altitude necessary to generate the kinetic energy estimated for each SUT. With the exception of the propeller, each of the items dropped would require a few hundred feet to approach terminal velocity. At flight altitudes lower than the provided fall distance, the velocity and kinetic energy upon impact would be reduced.

WINDMILLING EFFECT

The differences in kinetic energy of the disabled DJI Phantom 4 Pro with free-spinning propellers, with bound propellers, and without any propellers were rather significant. Kinetic energy was 35% higher with bound propellers and 85% higher with no propellers compared to the stock DJI Phantom 4 Pro with free-spinning propellers. These kinetic energy deltas due to propeller conditions were increased to 50% and 124%, respectively, when the quadcopter had a payload. The propellers added drag as the quadcopter fell regardless if they could spin or not, which led to the quadcopter without any propellers having the highest terminal velocity (and kinetic energy) of the three.

The increased terminal velocity and kinetic energy of the quadcopter with bound propellers, as compared to the free-spinning quadcopter, was attributed to a drag force being generated by *windmilling*, or the forced UAV propeller rotation driven by rushing wind as the UAV falls. Each quadcopter drop was performed with the UAV turned off, and the powered-down motor generated resistance to movement that had to be overcome before the windmilling was observed. During the drops with the stock DJI Phantom 4 Pro, the UAV fell for 1.23 ±0.02 seconds prior to the observation of windmilling. That fall time translates to fall distances of 22.5 to 23.9 ft (6.9 to 7.3 m) and UAV fall velocities of 35.4 to 36.3 ft/s (10.8 to 11.1 m/s). Recent literature published on quadcopter UAV collateral damage threats reported the absence windmilling (Reference 7). The contrasting results found in this study may be attributed to differences in drop distance in the test bed or the type of quadcopter dropped.

Windmilling reduced the projected terminal velocity and therefore strongly reduced the kinetic energy due to the dependence on the magnitude of the velocity squared as shown in Equation 5. The terminal velocity extrapolation from fall time assumed a constant drag coefficient applied to the UAV or UAV components as the object fell. This assumption may not be true for the windmilling contributions to the drag force since low fall speeds did not generate windmilling, and the volume/frequency of sound from windmilling produced a sweep towards higher volume and higher frequency during acceleration. The error in the constant drag coefficient assumption would generate larger drag in the falling quadcopter UAV at high velocities and therefore a lower terminal velocity and lower kinetic energy upon impact at terminal velocity.

The windmilling event also changed the orientation of the quadcopter UAV upon impact compared to the UAV fall without windmilling. If the disabled UAV was capable of windmilling (i.e., the propellers were still intact and free spinning), the UAV landed in the upright orientation. Researchers at the landing area level reported 7 out of 7 drops in which the windmilling DJI Phantom 4 Pro touched down with the landing gear making first contact. In contrast, none of the 7 drops of the DJI Phantom 4 Pro without propellers landed in the upright position. A bar graph of the impact angles is shown in Figure 3.

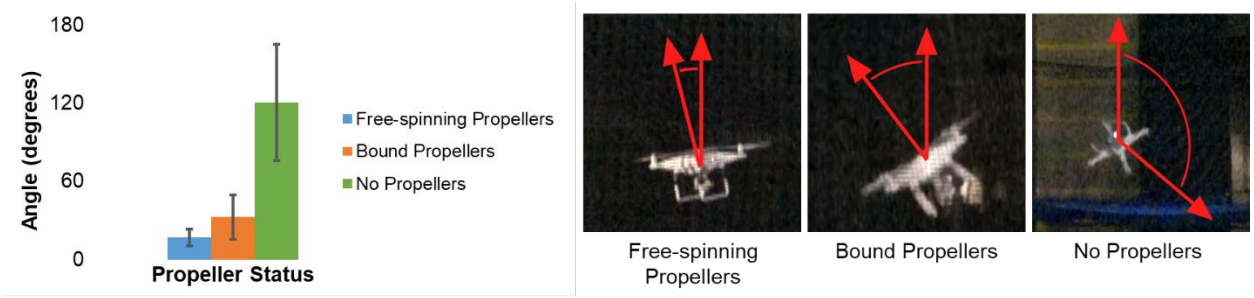

(a) Quadcopter impact angle. (b) High-speed still images from quadcopter drops.

FIGURE 3. Impact Angle of Falling Quadcopter at Test Bed Landing Area.

The data shown in Figure 3a represents the angle of each quadcopter from zenith. The data represents angular fits to still photographs pulled from high-speed video during the quadcopter drops (Figure 3b). The angle data presented in Figure 3 represents the average angle from all the fall tests that had usable video images: 11 tests with a quadcopter with free-spinning propellers, 10 tests with propellers bound, and 7 tests with quadcopters with no propellers. The angle was evaluated just before impact, which represented a ~94-foot (~28.7-meter) drop.

BC ANALYSIS

This study used the BC model to quantify the threat from each SUT. The governing BC model equation is shown in Equation 6. The model assumed the target was stationary relative to the projectile prior to impact. The BC model used the mass of the target and impact area to scale the kinetic energy of the projectile such that high kinetic energy projectiles with the smallest contact area produced the largest BC value.

$$Blunt\ Criterion\ (BC) = \ln\left(\frac{KE}{M^{\frac{1}{3}}TD}\right) \tag{6}$$

where KE is kinetic energy (J), M is mass of the struck object (skull) (Kg), T is combined thickness of the soft tissue and skull at impact location (cm), and D is diameter of contact area (cm).

This analysis assumed that a person was struck in the head by a SUT that had fallen far enough to reach terminal velocity. The probability of striking a person was not factored into the analysis, and only blunt force head strikes were considered due to vulnerable nature of the near-perpendicular surfaces of the head to a SUT falling vertically. Despite a significant injury risk, laceration injuries were not considered in this study due to a low probability of the laceration injury being lethal (Reference 8). For the BC calculations, several assumptions were made about the size and shape of the head that would be struck by the falling quadcopter. The head shape was a 7.09 in (18 cm) diameter sphere weighing 13.2 lb (6 kg) with combined skull and soft tissue thickness of 0.51 in (1.3 cm) (Reference 9).

CONTACT AREA ESTIMATES

The contact area between a human head and a disabled quadcopter was possible in two configurations depending on the orientation of the quadcopter at the time of impact: upright or rotated. In both orientations, the impact occurred between a skull and the deformable/frangible plastic components of the DJI Phantom 4 Pro. Due to the complex geometry of the quadcopter and probable deformation of the quadcopter body during the impact, the contact area was measured rather than calculated. The measurement was performed by dropping a DJI Phantom 4 Pro onto a witness Styrofoam head and then measuring the indentation left in the head after impact.

The collision between a Styrofoam head and the upright quadcopter resulted in the landing gear making contact with the head (see Figure 4). The upright orientation was observed at impact for DJI Phantom 4 Pro quadcopters when the propellers were free-spinning and therefore experienced windmilling. The landing gear deformed to match the curvature of the head and fractured at the interface between the landing gear and body of the quadcopter. The investigators did not observe direct contact between the head and the body of quadcopter during an upright orientation impact. The quadcopter's landing gear slid down the head, which resulted in rotation and deflection of the quadcopter. The indentation after impact has an area of 0.79 in^2 (5.1 cm^2) and produced a depth of 0.20 in (0.5 cm). The upright impact was not considered in the BC analysis because the analysis assumes a perfectly inelastic collision, but the upright quadcopter impact was only a partial kinetic energy transfer due to the deflection that avoided quadcopter center of gravity impact with the head.

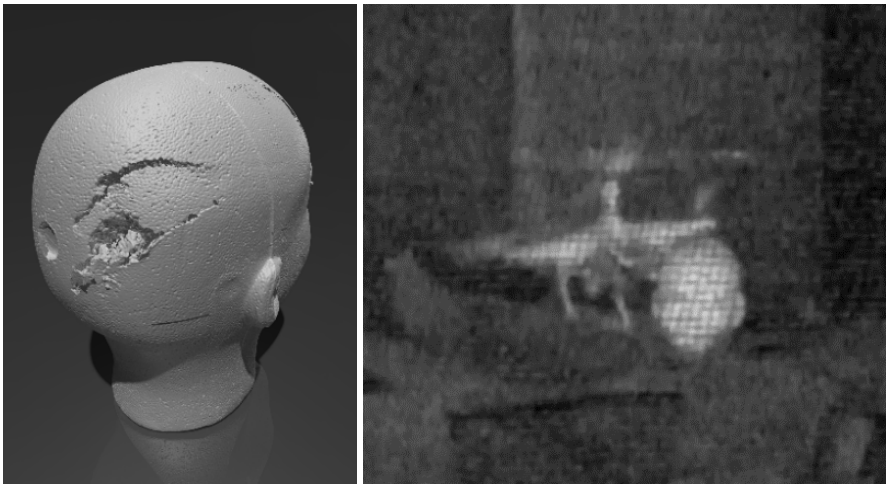

(a) Styrofoam head showing impact damage from an upright quadcopter.

(b) Still photograph from high-speed video of the impact.

FIGURE 4. UAV Landing Gear Colliding With Head.

The Styrofoam head impact with a rotated Phantom 4 Pro quadcopter, observed for quadcopter drops without windmilling, is shown in Figure 5. The rotated quadcopter impacted the Styrofoam head in the saddle between two propeller arms. The indentation after impact has an area of 4.3 in^2 (27.7 cm^2) and produced a depth of 0.43 in (1.1 cm). The impact resulted in a deflection of the falling quadcopter, but that was after a direct impact between the head and quadcopter body. The impact area witnessed on the Styrofoam head after impact with the quadcopter saddle was used for all of the BC calculations of quadcopter impact regardless of the orientation of the quadcopter because it was an observed impact with a large degree of kinetic energy transfer between the falling quadcopter and head.

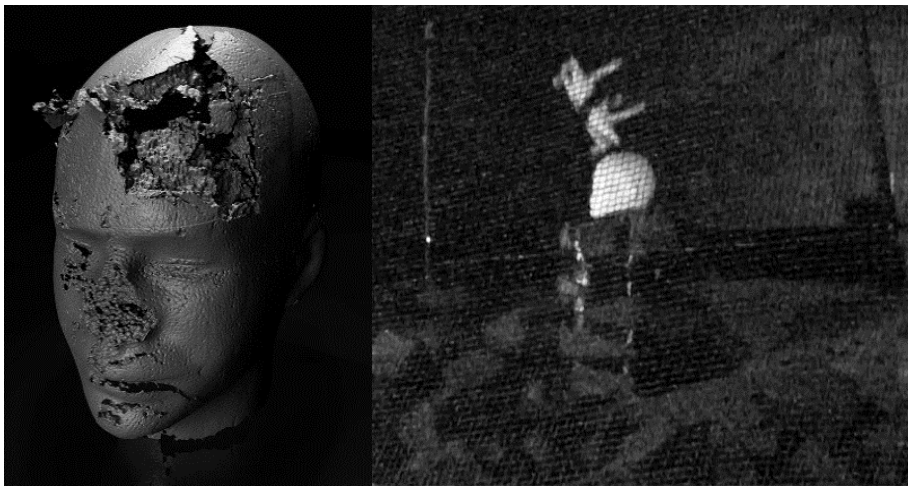

(a) Styrofoam head showing impact damage from rotated quadcopter.

(b) Still photograph of impact from high-speed video.

FIGURE 5. UAV Saddle Colliding With Head.

The DJI motor is shown in Figure 6. The motor was modified from its as-received state with a highly reflective tape, which made tracking the object easier as it fell. The motor was a dense, small aspect ratio cylinder with a hard metal casing. Due to the metal casing, this SUT was not assumed to have frangible/deformable character upon impact. The contact area was assumed to be the top of the cylinder, which produced a contact area of 0.95 in^2 (6.1 cm^2).

FIGURE 6. DJI Phantom 4 Pro Motor.

The DJI battery was dislodged from the UAV repeatedly during drop tests. Although significant force would be required to remove the motor or camera from the DJI Phantom 4 Pro, the battery removal threshold was comparatively lower. Therefore, a CUAV weapon attack would have a higher likelihood of separating the battery compared to the motor or camera. The Phantom 4 Pro uses a metal casing around the lithium polymer battery. Hard cases are commonly added to lithium polymer batteries to improve robustness during typical life cycle, but in this instance resulted in a hardened SUT with little frangible/deformable character upon impact.

Two orientations of the battery were considered for the impact between the battery and skull: side impact and corner impact. Geometrical limitations were applied to both orientations to derive the impact area as shown in Figure 7. The side of the battery is long enough that curvature of the head limits the contact area rather than the area available on the battery side, and a penetration depth would dictate the corner contact area. To estimate the surface area of a rectangular cuboid that would have contact with the head, the head was approximated as a sphere with a diameter of 7.09 in (18 cm) and a compression thickness of 0.51 in (1.3 cm). The compression thickness was the combined average thickness of the human skull and soft tissue and was used as the limit of intrusion because any additional depth would result in high probability of fatality brain injury (Reference 22). This analysis led to a contact area of 5.75 in^2 (37.1 cm^2) for the side of battery. The corner of the battery was again assumed to have a compression thickness of 0.51 in (1.3 cm). The impact area was estimated as the cross section of the battery flush with the head surface when the pyramidal corner of the battery penetrates the head compression thickness of 0.51 in (1.3 cm). This analysis resulted in a contact area of only 0.67 in^2 (4.3 cm^2) for the impact between the head and corner of the DJI battery.

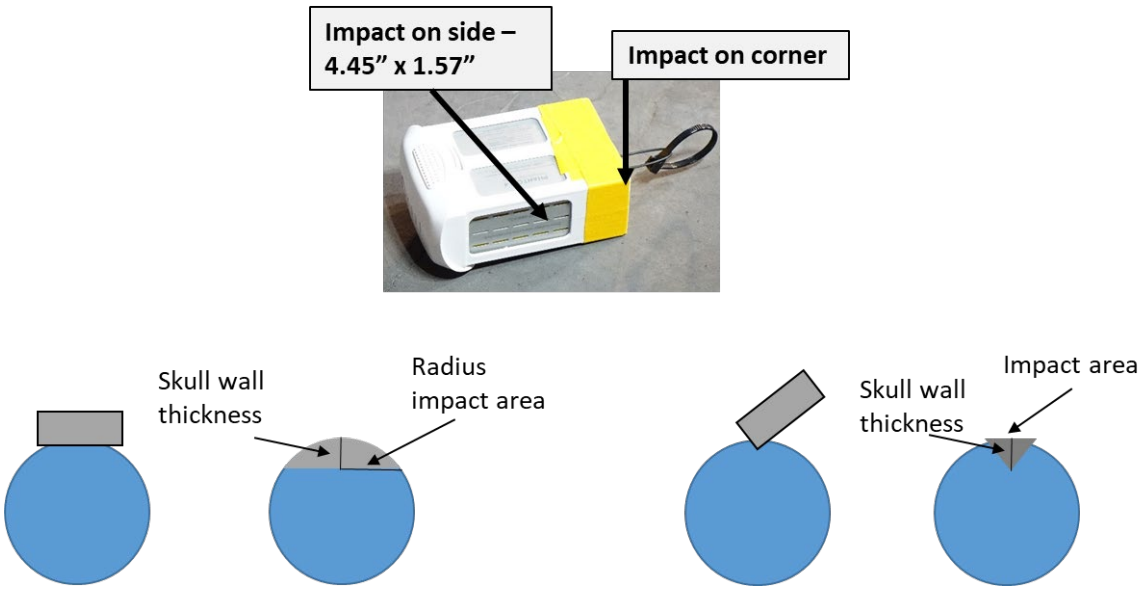

FIGURE 7. DJI Phantom 4 Pro Battery and Predicted Contact Area of Battery Side and Corner Impact With a Head.

The stock DJI camera is shown in Figure 8. The camera was a protuberance off the body of the quadcopter and therefore susceptible to removal during a CUAV weapon attack. The precise mass that would be removed during an attack as well as the region of the asymmetric camera assembly that may impact a head was expected to be highly variable. For the purposes of this investigation, the entire camera assembly was dropped. The area of the camera lens was used as the impacting surface since this surface was inherently a component of the camera that may be released from the quadcopter during an attack. Due to the camera appendage having a large percentage of glass and metal, this SUT was not assumed to have frangible/deformable character upon impact. The lens of the camera had a contact area of 1.4 in^2 (9.0 cm^2).

FIGURE 8. DJI Phantom 4 Pro Camera.

A payload-burdened DJI Phantom 4 Pro is shown in Figure 9. The range of possible payloads that could be attached to a modern quadcopter is exhaustive, from objects as inane as a beer bottle to objects as serious as a bomb. This investigation used a three-dimensional (3D)-printed 1.6-inch (40-millimeter) grenade surrogate weighing 0.66 lb (0.30 kg). The payload extended beyond the legs and camera of the DJI quadcopter. The payload therefore created a new contact surface—the inactive fuse assembly of the surrogate grenade. The contact surface of the payload was assumed to not have frangible/deformable character upon impact and had a contact area of 1.6 in^2 (10.3 cm^2).

FIGURE 9. Phantom 4 Pro With Custom Payload—Improvised Explosive Device (IED) Surrogate.

BC VALUES

The BC values for each SUT are shown in Table 2. The BC value provides a threat figure of merit that accounts for mass, terminal velocity, and contact area of the impact. In 2009, Raymond et al., extended the BC analysis to account for blunt force trauma to the head injuries and found that a BC value of 1.6 translated to a 50% probability of skull fracture (Reference 22). That correlation draws concerning questions about the dangers posed by all of the SUTs presented in Table 2: with the exception of the DJI motor, all of the SUTs had a BC value equal to, or greater, than 1.6. The additional drag of propellers slows the falling intact quadcopter with and without the payload attached. The reduction in terminal velocity was observed in a reduced kinetic energy and BC value, but the drag was not sufficient to reduce the BC value below 1.6 for the quadcopter with or without a payload. The DJI battery had the largest and smallest contact areas in the analysis: as would be expected, the corner strike of the battery posed a significantly higher threat (39%) than the side strike when evaluated in terms of BC value. The quadcopter with a protruding payload had the highest BC values based on both the high kinetic energy these threats would have upon impact at terminal velocity and the small surface across which the energy would transfer to a victim’s head.

TABLE 2. Impact Area and BC Value of SUT-Head Impact Assuming SUT Traveled at Terminal Velocity.

Falling Object	Impact Structure	Impact Area, in^2 (cm^2)	BC
Intact UAV – free-spinning propellers	Saddle	4.3 (27.7)	3.1
Intact UAV – 4 bound propellers	Saddle	4.3 (27.7)	3.4
UAV – no propellers	Saddle	4.3 (27.7)	3.7
DJI motor	End	0.95 (6.1)	1.4
DJI battery	Side	5.8 (37.4)	2.8
DJI battery	Corner	0.68 (4.4)	3.9
DJI camera	Face	1.4 (9.0)	1.6
DJI shell	Saddle	4.3 (27.7)	2.1
UAV w/ payload – free-spinning propellers	Fuse assembly	1.6 (10.3)	3.9
UAV w/ payload – 4 bound propellers	Fuse assembly	1.6 (10.3)	4.4
UAV w/ payload – no propellers	Fuse assembly	1.6 (10.3)	4.7

Caution should be taken when predicting the probability of injury from disabled quadcopters based solely on BC value analysis due to differences in the Raymond et al. projectile and the ones presented herein. The Raymond et al. study used a rigid 1.5-in (3.8-cm) diameter projectile (impact area of 1.7 in^2 [11.0 cm^2]), which would be not be frangible or deformable. The payload-burdened quadcopter and isolated components of the quadcopter may have reasonable approximation to this projectile, but the intact plastic quadcopter has rather different character. The intact quadcopter has contact surfaces that are both frangible and deformable. Evidence of alternative energy loss pathways in the DJI Phantom 4 Pro can be seen in Figure 10.

(a) Crumple deformation in the propeller arm.

(b) Ejected components.

(c) Fractured landing gear.

(d) Top/bottom body rift.

FIGURE 10. Permanent Damage Observed After Quadcopter Crash Events.

Figure 10 generalizes damage commonly observed in a sample of 15 crashed DJI Phantoms after a disabling in-flight CUAV attack. Figure 10a shows accordion-like folding in a deformed propeller arm; this deformation would absorb energy, which would then not be available for transfer in an impact. Figure 10b shows a quadcopter with parts that were ejected upon impact with the ground. The ejected parts would reduce the mass contributing to the total kinetic energy transferred at a single impact site and therefore reduce the severity. Figure 10c shows fracture in the frangible landing gear, and Figure 10d shows a shear shift between the top and bottom sections of the quadcopter body, creating a rift along large sections of the interface between them. The energy absorbed in the landing gear fracture and body rift generation would not be available for transfer in an impact.

These differences in projectile character among plastic UAVs and rigid projectiles used in human tolerance studies may account for the large discrepancies currently seen in literature surrounding the assignment of probability of injury/fatality due to quadcopter impact. In 2000, the US Army Range Commander's Council estimated that a SUT with 79 ft-lb (107.1 N-m) of kinetic energy would have a 90% probability of fatality after a head impact (Reference 10), while in 2017, Camplotettano et al. estimated a SUT with 114 ft-lb (154.6 N-m) of kinetic energy would have less than a 5% probability of catastrophic head injury (Reference 11). These stark differences in probability of fatality found in independent tests have been investigated recently in great detail (References 7 and 12). In 2017, Arterburn et al. was able to show that projectile character played a significant role in resulting injury after blunt force trauma by impacting crash test dummies with projectiles

made of wood and steel as well as a UAV (Reference 7). Despite the fact that all three projectiles had the approximately the same kinetic energy (~112 ft-lb [151.9 N-m]), the UAV gave less than 0.1% probability of head injury AIS2 or greater, while the wood and steel gave a 99% probability of head injury AIS2 or greater. AIS is the Abbreviated Injury Scale, which ranks injury between 1 and 6. AIS2 head injury was described as a superficial penetrating head injury intruding "≤2cm beneath the entrance." While an appropriate scaling factor to account for UAV physical character has not yet been adapted into a BC or other assessments based on projectile properties, the marked difference in behavior of rigid projectiles versus that of a quadcopter should be weighted into the evaluation of the threat of a disabled quadcopter after a CUAV weapon attack. Despite having a relatively high BC value, these recent investigations indicate that an intact UAV may pose less of a blunt force trauma threat than rigid projectiles such as the battery, camera, or payload.

CONCLUSIONS

The successful use of a CUAV weapon against an in-flight quadcopter would disable the quadcopter. Depending of the type of CUAV weapon, the disabled quadcopter would fall to the ground either (1) broken into many pieces, (2) intact and incapable of windmilling, or (3) intact and capable of windmilling. This study compared the theoretical threat posed by a disabled quadcopter in each of these end states that struck a person in the head at terminal velocity.

The individual quadcopter UAV components tested herein were composed of rigid materials that eliminate several energy loss pathways observed in the deformable/frangible plastic quadcopter body. Breaking the quadcopter into parts resulted in a multiplication of the number of projectiles falling down, and these rigid components each pose a significant threat to anyone struck in the head. For this reason, CUAV weapons that lead to UAV structural break-up generate more risk to people from a disabled quadcopter due to the possibility of multiple strikes on a single person or multiple people being struck.

Some of the disabled quadcopters tested were configured to allow the propellers to free-spin during the descent, which led to windmilling. The windmilling effect was observed for the stock DJI Phantom 4 Pro quadcopter after ~23 ft (7.0 m) of falling, and the additional drag generated through windmilling reduced the estimated terminal velocity and kinetic energy upon impact. In addition to producing drag, windmilling oriented the DJI quadcopter to land in an upright orientation. The upright orientation led to first contact during impact to be with the landing gear for a stock DJI Phantom 4 Pro, which introduced energy absorption mechanisms such as deformation and fracture of landing gear. The upright orientation also generated structural hindrance for impact between the quadcopter center of gravity and head. If a quadcopter were to be intentionally disabled above people, a motor shutdown mechanism that allowed the disabled quadcopter to windmill would be the recommended approach to minimize possible blunt trauma head injury.

REFERENCES

1. Federal Aviation Administration. *FAA Aerospace Forecast - Fiscal Years 2017 - 2037*, 2017.

2. D. B. Larter. "SOCOM Commander: Armed ISIS Drones Were 2016's 'Most Daunting Problem'," *Defense News*. https://www.defensenews.com/digital-show-dailies/sofic/2017/05/16/socom-commander-armed-isis-drones-were-2016s-most-daunting-problem/

3. D. Ernst. "Gang Used Swarming Drones to Attack FBI; 'High-speed' Passes Targeted Hostage Rescue Team," *The Washington Times.* https://www.washingtontimes.com/news/2018/may/3/gang-used-swarming-drones-to-attack-fbi-high-speed/

4. B. Jansen. "FAA Prohibits Drone Flights Over Federal Prisons, Coast Guard Bases," *USA Today*. https://www.usatoday.com/story/news/2018/06/26/faa-bans-drone-flights-over-prisons-coast-guard-bases/733734002/, retrieved 4 October 2018.

5. V. Staff. "Idiots with Drones Shut Down the UK's Second Largest Airport—Again," *The Verge*. https://www.theverge.com/2018/12/20/18149819/london-gatwick-airport-drone-shutdown-reports

6. D. Grossman. "Drones are (Still) a Firefighter's Nightmare," *Popular Mechanics*. https://www.popularmechanics.com/flight/drones/a21599465/drones-interrupt-fire-fighting-wildfires/

7. University of Alabama. *Final Report for the FAA UAV Center of Excellence Task A4: UAV Ground Collision Severity Evaluation Revision 2*, by D. Arterburn, M. Ewing, R. Prabhu, F. Zhu, and D. Francis. Huntsville, AL, ASSURE, University of Alabama, 2017.

8. D. Arterburn, C. Duling, and N. Goli. "Ground Collision Severity Standards for UAS Operating in the National Air System (NAS)," *17th AIAA Aviation Technology, Integration, and Operations Conference*, Denver, CO, 2017.

9. D. Raymond, C. Van Ee, G. Crawford, and C. Bir. "Tolerance of the Skull to Blunt Ballistic Temporo-parietal Impact," *Journal of Biomechanics*, Vol. 42, 2009, pp. 2479-2485.

10. Range Commander's Council Range Safety Group. *Common Risk Criteria for National Test Ranges: Inert Debris (Standard 321-02)*, 2000.

11. E. T. Campolettano, M. L. Bland, R. A. Gellner, D. W. Sproule, B. Rownon, A. M. Tyson, S. M. Duma, and S. Rowson. "Ranges of Injury Risk Associated With Impact for Unmanned Aircraft Systems," *Annals of Biomedical Engineering*, Vol. 45, No. 12, 2017, pp. 2733-2741.

12. Center for the Study of the Drone at Bard College. "Drone Registrations – A Preliminary Analysis," by D. Gettinger and A. H. Michel. Annandale-on-Hudson, NY, November 2017. https://dronecenter.bard.edu/projects/other-projects/drone-registrations/, retrieved 4 October 2018.

13. University of Alabama. *Final Report for the FAA UAS Center of Excellence Task A11 – Part 107 Waiver Request Case Study*, by D. Arterburn. Huntsville, AL, ASSURE, University of Alabama, 2016.

14. Monash University. "Human Injury Model for Small Unmanned Aircraft Impacts," by Civilian Aviation Safety Authority. Melbourne, Australia, 2013.

15. Naval Air Warfare Center Aircraft Division. "Crash Lethality Model," by J. A. Ball, M. Knott, D. D. Burke. Patuxent River, MD, NAWCAD, 2012.

16. European Aviation Safety Agency. *"Drone Collision" Task Force Final Report*, 2016.

17. A. Washington, R. Clothier, J. Silva. "A Review of Unmanned Aircraft System Ground Risk Models," *Progress in Aerospace Sciences*, Vol. 95, 2017, pp. 24-44.

18. Z. Skobir and T. Magister. "Assessment of a Light Unmanned Aircraft Ground Impact Energy," *Promet - Traffic & Transportation*, Vol. 23, No. 2, 2011, pp. 97-104.

19. A. V. Shelley. "A Model of Human Harm From a Falling Unmanned Aircraft: Implications for UAS Regulation," *International Journal of Aviation, Aeronautics, and Aerospace*, Vol. 3, No. 3, 2016.

20. MITRE Corporation. "Modeling Risk-Based Approach for Small Unmanned Aircraft Systems," McLean, VA, 2017.

21. MITRE Corporation. "A New Paradigm for Small UAS," McLean, VA, 2012.

22. P. Wu and R. Clothier. "The Development of Ground Impact Models for the Analysis of the Risks Associated With Unmanned Aircraft Operations over Inhabited Areas," *Proceedings of the 11th Probabilistic Safety Assessment and Management Conference*, Annual European Safety and Reliability Conference, 2012.

INITIAL DISTRIBUTION

1 Defense Technical Information Center, Fort Belvoir, VA

ON-SITE DISTRIBUTION

1 Code DC12100 (file copy)
2 Code D5J4000 (archive copies)
1 Code D55J500, Sechrist, Z.